GEOCHEMISTRY

Early diagenetic control on the enrichment and fractionation of rare earth elements in deep-sea sediments

Yinan Deng[1,2,3], Qingjun Guo[4,5]*, Congqiang Liu[6], Gaowen He[1,2], Jun Cao[1,2], Jianlin Liao[7], Chenhui Liu[1], Haifeng Wang[1], Jianhou Zhou[1], Yufei Liu[1], Fenlian Wang[1], Bin Zhao[1], Rongfei Wei[4], Jiang Zhu[3], Haijun Qiu[1]

The rare earth elements and yttrium (REY) in bioapatite from deep-sea sediments are potential proxies for reconstructing paleoenvironmental conditions. However, the REY enrichment mechanism and the reliability of this tracer remain elusive because of the lack of key information from ambient pore water. Here, we report high-resolution geochemical data for pore water, bottom water, and bioapatite from deep-sea sites in the western Pacific. Our results reveal that the benthic flux of REY from the deep sea is less substantial than from the shallow marine realm, resulting in REY-rich sediment. The depth distribution of REY in pore water is opposite to that of bioapatite, and REY patterns and neodymium isotopic compositions are not uniformly distributed within bioapatite. These results indicate alteration of REY and neodymium isotopic compositions during early diagenesis. Therefore, we infer that REY from bioapatite are not robust recorders of the deep marine environment through Earth's history.

INTRODUCTION

Rare earth elements (REEs) and yttrium, referred to as REY, are robust proxies of seawater processes (*1*). REY are of increasing economic interest as an important strategic resource (*2*). In particular, heavy REE (HREE; Gd-Lu) are more valuable because of their limited reserves being essential for modern high-technology products (*3*). Investigating potential HREE resources is thus a subject of considerable interest, considering that exploring feasible deposits still faces substantial challenges. The most HREE-rich materials in the world are deep-sea sediments (termed REY-rich muds) (*4*–*6*). These deposits are not only currently identified in the Pacific (*4*–*8*) but recently also reported from the Indian (*9*) and northern Atlantic (*10*) oceans.

From the explorative/oceanographical perspective, the knowledge gap that needs addressing is the origin and accumulation mechanism of the REY-rich muds. There is consensus that apatite is the eventual host of REY in deep-sea sediment (*7*, *8*, *11*). The types of apatite in marine sediments are bioapatite (fish debris, i.e., teeth and bones) (*7*), authigenic carbonate fluorapatite, and detrital apatite (igneous or metamorphic origin) (*12*, *13*). Although bioapatite is not super abundant in the sediments, it can hold at least ~69% of the total REY of REY-rich muds in the Pacific (*9*). Authigenic carbonate fluorapatite could also be responsible for REY enrichments in sediment, but this only occurs in limited geological settings such as near to mid-ocean ridges (*5*). However, the source of REY in sediment is still a matter of debate. It has been suggested that REY in deep-sea sediments originates from mid-ocean ridge hydrothermal fluids (*4*). However, the low concentrations of REY and positive Eu anomaly (*14*) observed in hydrothermal fluid display markedly different features from deep-sea sediments. Nonetheless, hydrothermal activity represents a source of Fe-Mn (oxyhydr)oxides, which play an important role in the formation of authigenic apatite and the accumulation of REY in the sediment (*5*). REY in deep marine settings have been suggested to have a seawater origin (*5*, *15*), but other studies have pointed out that the diffusion of REY from seawater into bioapatite is too slow to produce such high accumulations of REY (*11*, *16*), implying that REY-rich pore water may be the source. Dissolution of marine particles causes REY to be adsorbed onto bioapatite during early diagenesis, confirming that pore water is the principal source of REY in deep-sea sediments (*5*, *8*, *11*, *17*, *18*). To the best of our knowledge, there has been little attention paid to REY of pore water in REY-rich muds, contributing to the lack of understanding of the sources and mechanisms responsible for the accumulation of REY in deep-sea sediments.

REY and Nd isotopic signatures of bioapatite within marine sediments are also widely used for reconstructing paleoseawater conditions and processes (*11*, *15*, *18*, *19*). However, bioapatite commonly becomes enriched in REY after deposition, suggesting that REY in bioapatite may record diagenetic conditions rather than a pristine seawater signal (*16*, *17*, *20*). Because of the differences in the distributions of REY in pore water and seawater (*21*–*25*), a new framework that accounts for REY in pore water from different depositional environments is needed to enable REY to be used as a paleoceanographic tracer (*20*). Toyoda and Tokonami (*11*) revealed that bioapatite from shallow sea sediments appears to be an unreliable archive for seawater. Existing data about REY of pore water are mainly from the shallow marine realm. By contrast, investigations of REY in pore water at deep-sea sites are scarce (*18*), particularly in deeper subsurface pore water. Moreover, understanding the relationship of the REY in bioapatite, bottom water, and the surrounding pore water is of great importance in revealing the reliability of REY as a paleoceanographic tracer. However, no study dedicated to the REY geochemistry of all these three phases has been conducted to date.

[1]MNR Key Laboratory of Marine Mineral Resources, Guangzhou Marine Geological Survey, Guangzhou 510075, China. [2]Southern Marine Science and Engineering Guangdong Laboratory (Guangzhou), Guangzhou 511458, China. [3]Research Center for Earth System Science, Yunnan University, Kunming 650091, China. [4]Institute of Geographic Sciences and Natural Resources Research, Chinese Academy of Sciences, Beijing 100101, China. [5]College of Resources and Environment, University of Chinese Academy of Sciences, Beijing 100049, China. [6]Institute of Surface-Earth System Science, Tianjin University, Tianjin 300072, China. [7]School of Earth Sciences and Engineering, Sun Yat-sen University, Guangzhou 510275, China.
*Corresponding author. Email: guoqj@igsnrr.ac.cn

Here, we present high-resolution REY data of pore water, bottom water, and bioapatite from REY-rich muds in the western Pacific (Fig. 1). The present study provides new insight into the origin and detailed accumulation processes of REY enrichment in sediment. In addition, it provides direct evidence pertaining to the use of REY in deep-sea bioapatite as a paleoceanographic proxy.

Geological background

GC08, GC062, and GC120 sites were cored in the Pigafetta Basin, western Pacific (Fig. 1). The sediments at 0 to 40 m beneath the seafloor are dominated by brown zeolitic clay, at water depths between 5000 and 6500 m. They exhibit a low sedimentation rate (<0.5 m/million years) (*26*) and low organic matters contents and contain terrigenous clastic material. This area is surrounded by Magellan seamounts, Marcus-Wake seamounts, and Marshall Islands (*18*). In general, the upper parts of the GC08 site (ca. 742 cm in thickness), GC062 site (ca. 800 cm in thickness), and GC120 site (ca. 700 cm in thickness) consist of siliceous clay showing high water content, whereas the middle to lower parts are dominated by pelagic clay with relatively low water content.

RESULTS

The REY, major elements, anion, cation, and Nd isotope data are listed in tables S1 to S5. REY concentrations in pore water range between 289 and 15,363 pM. Significant variability of REY in pore

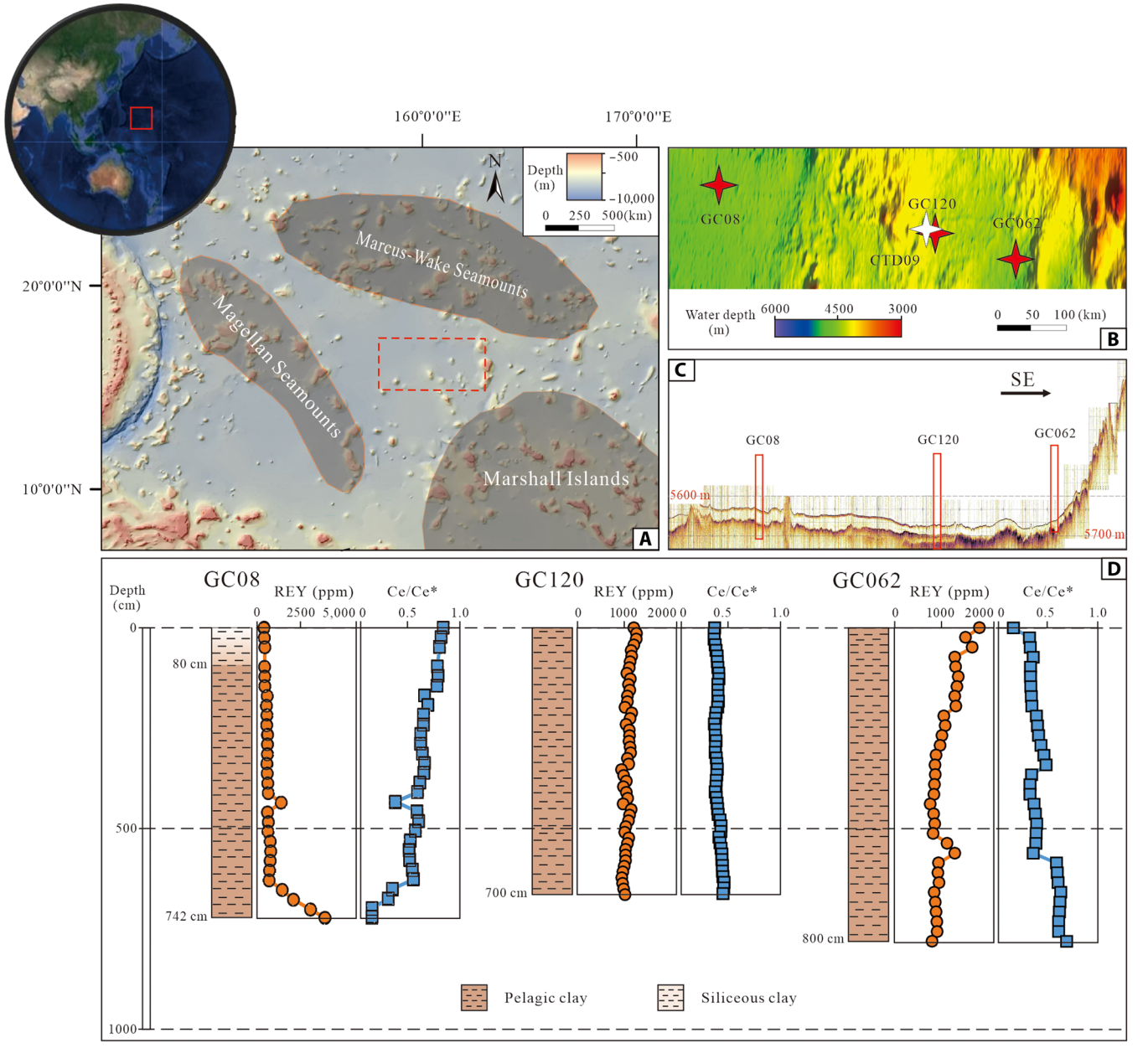

Fig. 1. Location, bathymetry, and lithological columns of the sampling area. (**A**) Research area located in Pigafetta basin, western Pacific Ocean. (**B**) High-resolution bathymetry maps of the study area. (**C**) The seismic sub-bottom profile of GC08, GC120, and GC062. (**D**) The lithological columns, REY, and Ce/Ce* of deep-sea sediments.

water was observed at GC062 site (~2620 to 15,363 pM), with the smallest variability observed at site GC08 (~289 to 5519 pM). Ce/Ce* values of the pore water samples range from 0.18 to 0.65 (mean = 0.40 ± 0.12, n = 90) and middle REE (MREE)/MREE* range from 0.27 to 0.54 (mean = 0.38 ± 0.06, n = 90). On the basis of elevated REY concentrations in the seawater and pore water REY profiles of all sites, the REY release from sediments mainly occurs in two intervals: (i) a weaker release at sediment-water interface (SWI) and (ii) a relatively strong release in deep subsurface sediment (Fig. 2). REY concentrations in pore water are up to 12,025 pM at SWI, two orders of magnitude higher than in bottom seawater (558 pM). The deep subsurface shows substantial increases in pore water REY (the second REY-release event) at sites GC08 [~125 to 670 cm below the seafloor (cmbsf)], GC062 (~275 to 525 cmbsf), and GC120 (~200-550 cmbsf), consistent with removal of pore water REY in the lower part of the cores. Similar trends were observed for the MREE/MREE* values (Fig. 2). Mn, Fe, Al, NO_3^-, and SO_4^- in pore water remain nearly constant down cores, whereas Mn and NO_3^- show gradually decreasing concentrations with depth at GC08 site (Fig. 3).

Whole-rock samples show a high ΣREY from 368 to 3436 parts per million (ppm; mean = 961 ± 400 ppm, n = 111), indicating REY enrichment in sediment. Ce/Ce* values of the whole-rock samples range from 0.12 to 0.84 (mean = 0.45 ± 0.14, n = 111). Bioapatite samples show a greater ΣREY range from 15 to 16,739 ppm (mean = 4845 ± 4063, n = 101) than that of the sediment at the GC062 site. Almost all bioapatite fossils presented herein show distinct negative Ce anomalies (Ce/Ce* = 0.01 to 0.20, mean = 0.08 ± 0.05, n = 101), insignificant positive Eu anomalies, positive Y anomalies, and slight HREE enrichments. The REY of bioapatite at the GC062 site show

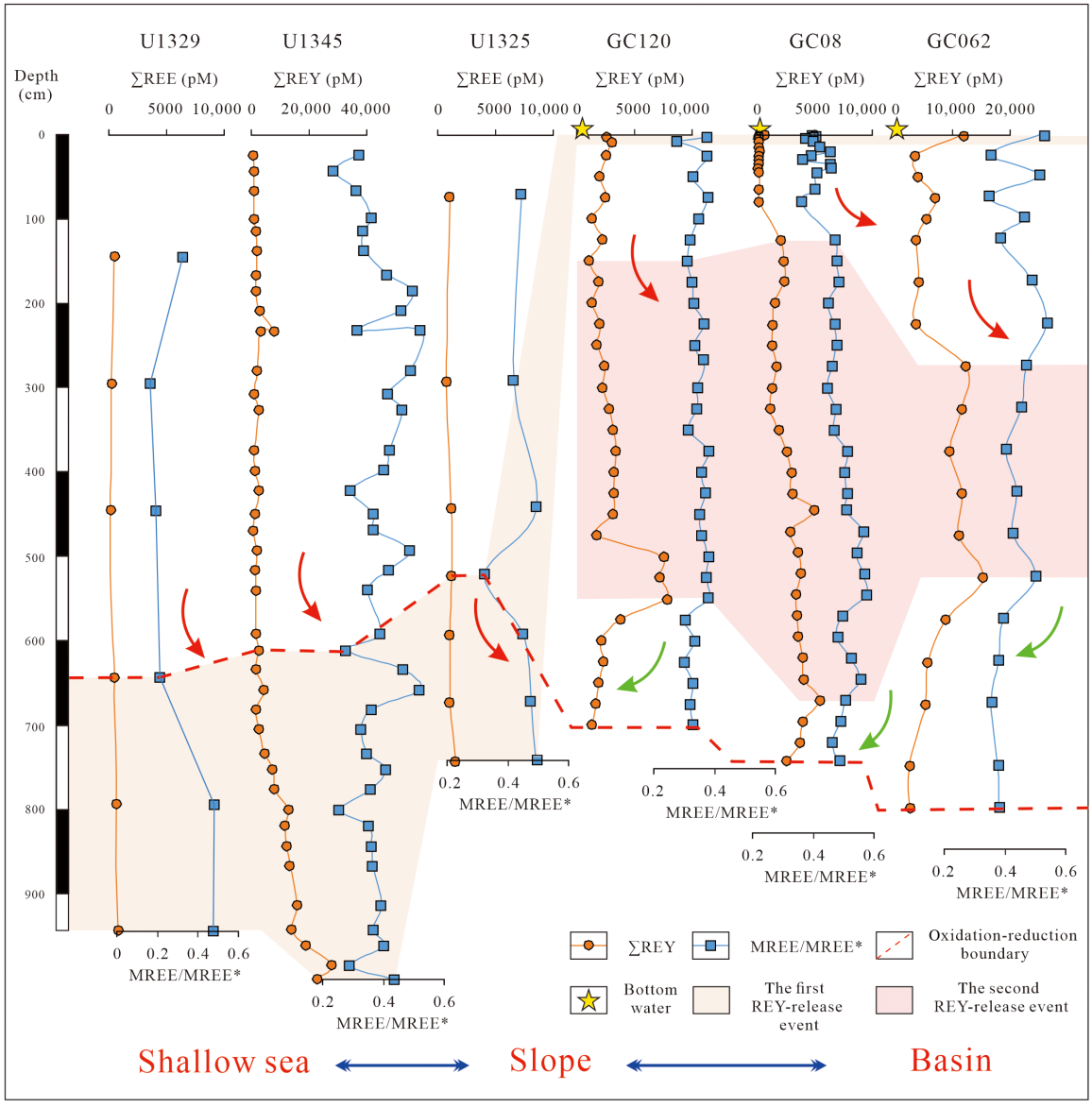

Fig. 2. Comparison of REY and MREE/MREE* variations in pore water from different sites ranging from shallow sea to slope to basin. Data sources: U1325 and U1329 sites (*36*) and U1345 site (*37*).

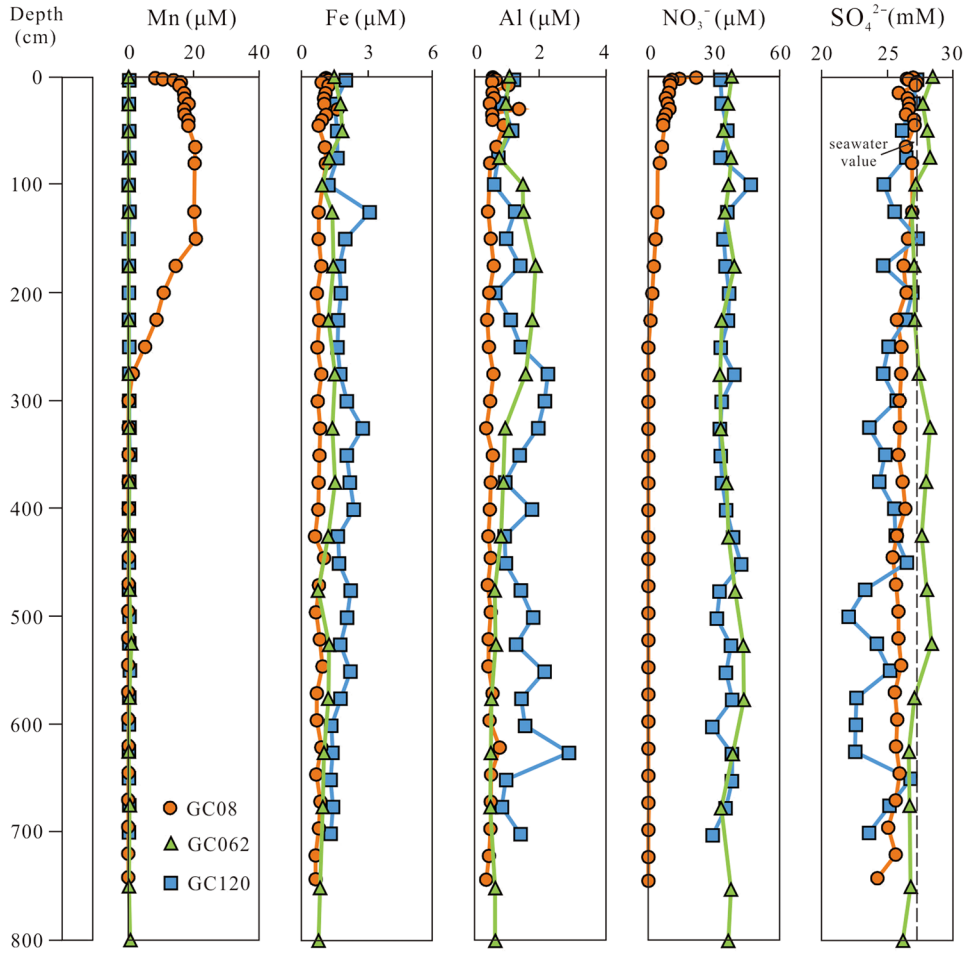

Fig. 3. Variations of Mn, Fe, Al, NO_3^-, and SO_4^{2-} in pore water at sites GC08, GC062, and GC120, western Pacific.

abruptly increasing concentrations from SWI (mean = 3145 ppm, n = 17) to 200 cmbsf layer (mean = 6455 ppm, n = 14), thereafter remaining constant down core. REY geochemistry is not uniformly distributed within a single bioapatite fossil and shows substantial variation from the root (outer rims) part to the tip (inner) part. The average concentrations of REY at the root part, middle part, and tip part in fossil teeth are 6808 ppm (~20 to 16739 ppm, n = 30), 5163 ppm (~16 to 13,759, n = 40), and 2534 ppm (~15 to 7947 ppm, n = 31), respectively. Ce/Ce* values decrease slightly from root part (mean = 0.10 ± 0.04, n = 30) to middle part (mean = 0.08 ± 0.03, n = 40) to tip part (mean = 0.06 ± 0.05, n = 31).

Similarly, the bioapatite fossil does not show a homogeneous εNd value and displays a large range of εNd values within individual samples. At GC062 site, bioapatite εNd values range from −12.0 to −1.4 (mean = −6.1 ± 2.9, n = 48), but the average εNd value becomes higher from root part (−6.7 ± 2.9, n = 19) and middle part (−6.7 ± 3.0, n = 16) to tip part (−4.6 ± 2.3, n = 13). Bioapatite has relatively higher εNd values in shallow sediment (≤100 cmbsf), where the average values of the root part, the middle part, and the tip part of fish teeth are −5.4 (n = 8), −4.3 (n = 5), and −3.3 (n = 6), respectively. The average εNd values of bioapatite become higher from the root part (−7.6, n = 11) and middle part (−7.7, n = 11) to tip part (−5.7, n = 7) at depth (≥100 cmbsf).

DISCUSSION

Role of deep-sea sediment in governing the oceanic REY budget

Pore water REY concentrations observed in this study are significantly higher than the previously published data (*18*, *20*–*23*, *25*). The high pore water REY favors the formation of REY-rich bioapatite due to the progressive diagenetic uptake of pore water REY by bioapatite in sediments (*16*). This process is controlled by the availability of REY in the pore water (*8*). Although REY in pore water are 100 times more concentrated than in seawater, the formation of such high accumulations of REY in bioapatite requires an unrealistically high flux of pore water through the sedimentary column (*11*) and a low sedimentation rate (*18*). It is suggested that the dominant process of adsorption occurs at the SWI and in the shallow burial environment (*15*, *17*, *27*). In addition to the SWI, there is an intensified enrichment area in deep (>1 m) burial environments, as demonstrated in later sections.

Two distinctive REY-release events are discernible in the seawater and pore water profiles. The first one occurs at the SWI and the second one that takes place in deeper subsurface sediments (Fig. 2). Two REY-release events lead to the REY enrichment of bioapatite because of subsequent transfer of REY to bioapatite. Pore water Nd concentrations rise near the SWI but undergo a steep fall down

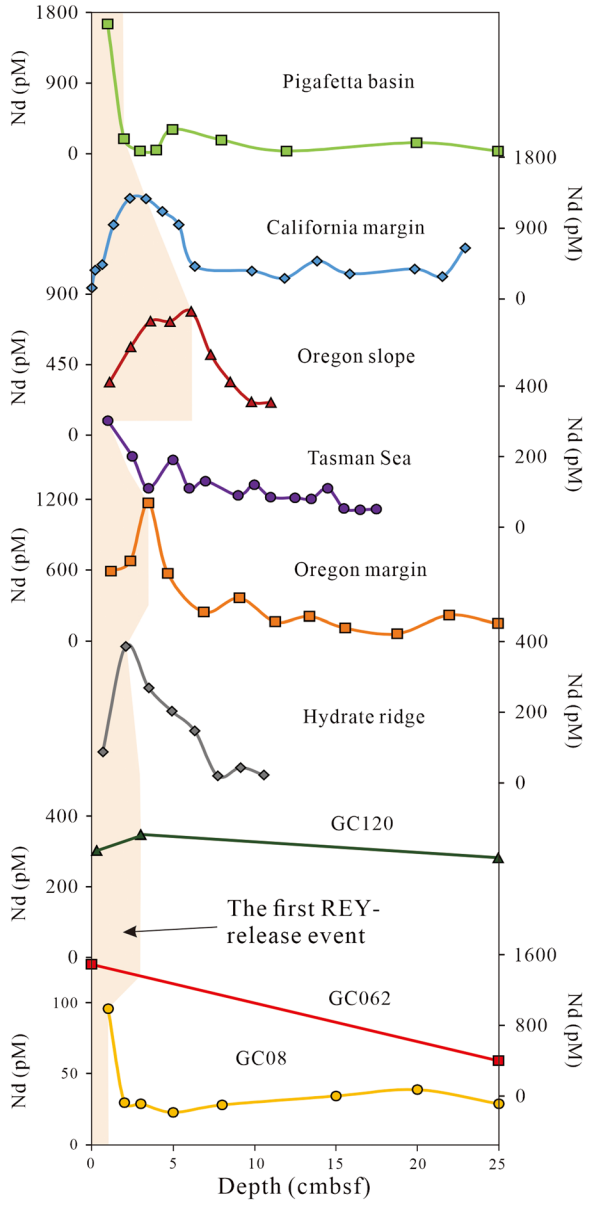

Fig. 4. Comparison of pore water Nd variations in global ocean. Data sources: California margin (*23*), Oregon margin (*24*), Oregon slope (*35*), Hydrate ridge (*59*), Pigafetta basin (*18*), and Tasman Sea (*20*).

core, which is consistent with the modern marine shallow-water subsurface environment of the seafloor (Fig. 4). The release of REY is thought to be controlled mainly by different redox conditions, i.e., oxic degradation of organic matter (*23*, *28*), reductive dissolution of Fe-Mn (oxyhydr)oxides (*23*, *29*), and dissolution of clay minerals (*30*). The redox conditions are controlled mainly by the input of organic matter, oxygen flux, and sedimentation rate (*31*). The dissolved Mn and Fe show relatively low concentrations, and dissolved Al concentrations remain nearly constant downward at GC062 and GC120 (Fig. 3), pointing to oxic conditions throughout the sediments without reduction of Fe-Mn (oxyhydr)oxides (*17*) and dissolution of clay minerals (*30*). Oxic conditions are also evidenced by seawater-like SO_4^{2-} concentrations and relatively high concentrations of NO_3^- (equal to or exceeding that of seawater; Fig. 3) (*31*). However, dissolved Mn enrichment with a peak concentration at 150 cmbsf and nearly constant dissolved Fe concentrations are shown in GC08, indicating the possible presence of suboxic conditions at intermediate depths (Fig. 3). The production zone of dissolved Mn does not match the peak REY concentrations, which is consistent with the suggestion that Mn oxides are not a principal carrier of REY (*23*). A stepwise decrease in NO_3^- concentrations in the shallow subsurface of core GC08 implies relatively low concentrations of dissolved oxygen in deeper sediment. The nonanoxic environments support the previous suggestion that O_2 penetrates much deeper in pelagic sediments of the Pacific Ocean (*32*–*34*).

The most reasonable explanation for pore water REY enrichment during the first REY-release event is the oxic degradation of organic matter (*18*, *28*), which mainly occurs near SWI under very low sediment accumulation rates (*32*, *34*). This interpretation is supported by the extremely low sedimentation rate of <0.5 m/million years in the study area (*35*). Recent studies emphasized a substantial benthic source of REY from seafloor to the global ocean, which can be regarded as a dominant contributor to the oceanic REY budget (*25*, *30*). Existence of upward diffusion of REY owing to the gradient between the pore water and bottom water REY concentrations (table S1), which show high observed pore water REY concentrations at <3 cmbsf, implies that pelagic sediments may still be a source of REY to the ocean. However, except for the GC062 site, which is probably influenced by detrital components from nearby seamounts (Fig. 1) (*18*), pore water REY concentrations near SWI at sites of GC08 and GC120 are relatively lower than previously published data from the shallow sea, slope, and calcareous deep-sea sediments (Fig. 4). These results are inconsistent with the recent assessment that pelagic sediments contribute the greatest benthic flux of REY to seawater (*20*, *24*). We infer that only insignificant amount of REY diffuses from pore water to the overlying water column in deep-sea area in the western Pacific, facilitating the accumulation of REY in the sediment column. The insignificant benthic source of REY to the global ocean might contribute to the enrichment of REY in pelagic muds.

REY-release event in deep burial environments

The second REY-release event and high values of MREE/MREE* were observed in the deep subsurface at research sites (Fig. 2). The results are similar to previously published REE data of pore waters at depth (>100 cmbsf) in the Cascadia margin (U1325 and U1329) (*36*) and the Bering Sea Slope (U1345) (*37*). The result suggests that the REY release from sediments and subsequent transfer into bioapatite during early diagenesis can occur in deep subsurface environments, comparable with previous results showing bioapatite REY enrichment, which develops at the SWI and intensifies systematically with depth (*8*, *16*).

Pore water REY enrichments in the California margin is caused mainly by the reduction of Fe oxides (*23*). A general absence of anoxic conditions was observed at our study sites. Given that most organic matter would be oxidized within the uppermost sediments (*18*), the mechanisms accounting for the desorption of REY in deeper oxic sediments remain poorly constrained. It is probably induced by the transformation of Fe minerals from the initial precipitates (i.e., ferrihydrite) to secondary minerals (i.e., goethite), which tends to reduce the reactive surface area, resulting in the release of REY to pore water (*38*). This explanation is mainly applicable to the region near the mid-ocean ridge where the influence of hydrothermal Fe-Mn

(oxyhydr)oxides is notable (*5*). However, the source of the terrigenous sediment in study area is dominated by aeolian dust (*6*). The transition from initial Fe precipitates to Fe smectite is an alternative explanation for the substantial release of adsorbed REY into nonanoxic pore water. The formation of montmorillonite as a result of interaction between Fe-Mn (oxyhydr)oxides and biogenic opal is favored over a large-scale sea area (*5*, *39*). This phenomenon is likely to result in the release of REY into pore water during the transformation to Fe smectite owing to large ionic radii of REY inhibiting their incorporation in the smectite structure (*5*). This inference is supported by the increasing amount of montmorillonite with depth in the study area (table S3).

The rise of MREE/MREE* values of study sites during the second REY-release event indicates that MREE are released preferentially from solid phases into pore water (Fig. 2). The post-Archean Australian shale (PAAS)-normalized REY distribution patterns of these pore water samples display slight MREE enrichment (Fig. 5, A, C, and E) compared to pore waters above and below this depth zone. This contrasts with the distinctive seawater pattern showing a progressive enrichment toward HREE and Ce depletion (Fig. 5, B, D, and F). Despite the "MREE bulge"–type pattern observed because of the reduction of Fe-Mn (oxyhydr)oxides under anoxic conditions (*23*, *25*), most modern marine pore waters do not show such extreme MREE enrichments under either oxic or anoxic conditions (*18*, *21*, *23*, *37*, *40*). The observed MREE enrichments in the [REE] pool of pore waters were due to the surface charges of Fe and Mn oxyhydroxides, which preferentially scavenge dissolved MREE from the water column that are subsequently released during early diagenesis (*41*).

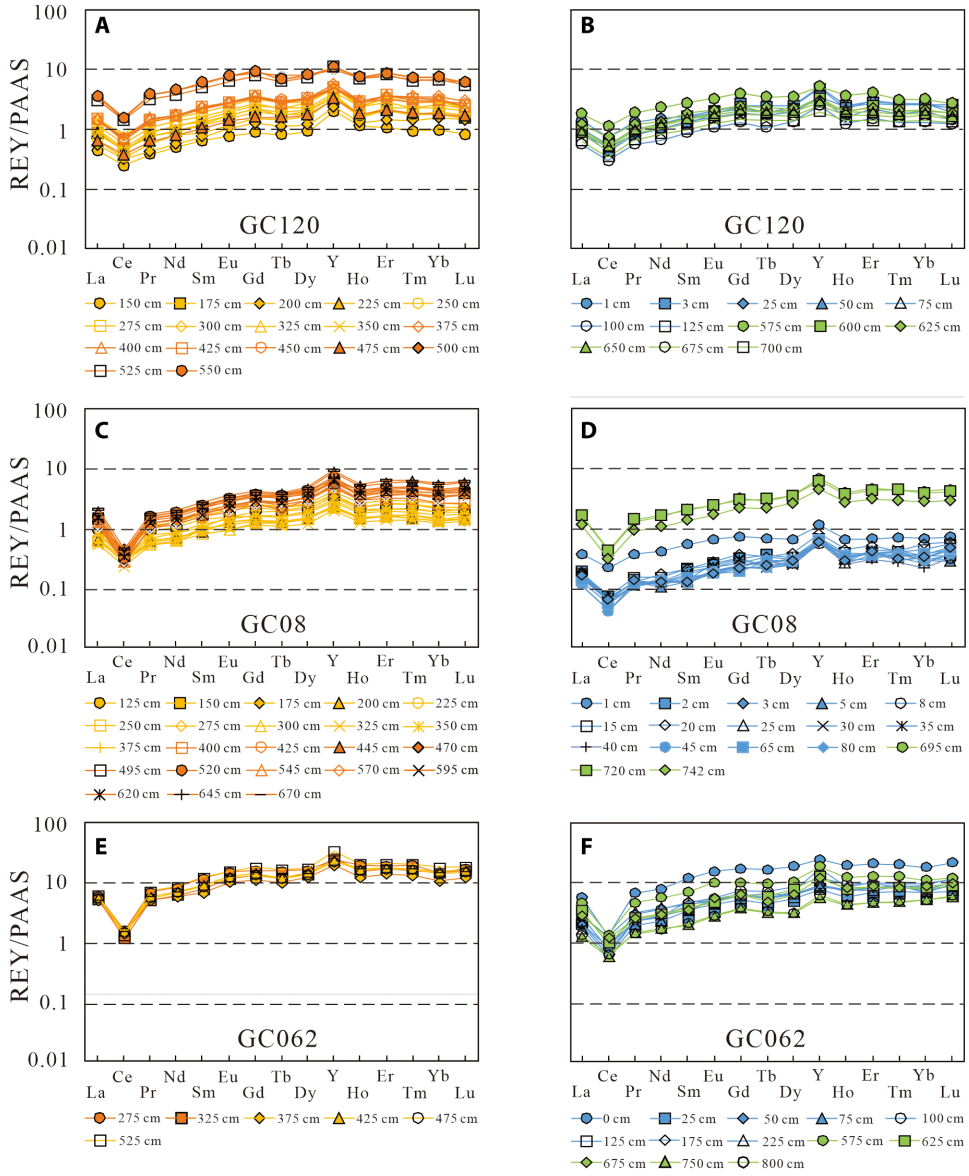

Fig. 5. PAAS shale-normalized REE distribution spectra of pore water from deep-sea sediment, western Pacific. (**A**, **C**, and **E**) The slight MREE enrichment patterns of pore water in the second REY-release event. (**B**, **D**, and **F**) The seawater-like REY patterns of pore water. The blue and green lines indicate pore water depth zone above and below the second REY-release event.

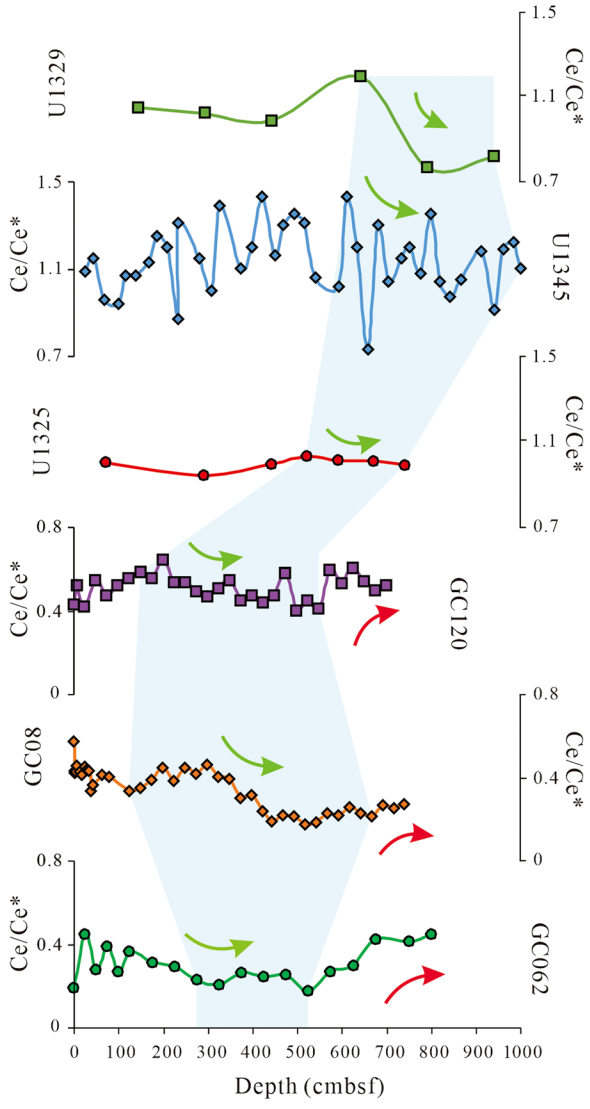

Fig. 6. Comparison of Ce/Ce* variations in pore water at the different sites from shallow sea to slope to basin. Data sources: U1325 and U1329 sites (*36*) and U1345 site (*37*).

As an element with multiple valence states, cerium (Ce) can exist in either trivalent or tetravalent forms depending on the environment and so is frequently used to assess redox conditions (*1*, *21*). The significant negative Ce anomalies in the sites range from 0.18 to 0.65 (table S1) are mainly due to oxic or suboxic conditions in the study area. The high values of Ce/Ce* in the shallow subsurface (Fig. 6) are likely derived from the decomposition of organic matter, as settling organic matter particulates preferential release Ce relative to other light REEs (LREEs) into pore water during its degradation near SWI (*18*, *23*). Furthermore, lower Ce/Ce* values are common in the second REY-release event at our study sites, consistent with the observation in Cascadia margin (*36*) and the Bering Sea Slope (Fig. 6) (*37*). The mechanism that leads to the removal of dissolved Ce from deep pore water under oxic-suboxic conditions remains unclear. Considering that there is little redox-related modification, the change of Ce/Ce* values is not only caused by the changing concentration of dissolved Ce but also caused by variations in the concentrations of the other REY (*9*). The variability of Ce/Ce* values can be explained by a mineralogical control (*42*), because the trivalent REY is linked to phosphate or Fe phases, while Ce are likely associated with Mn phases (*8*, *42*). Therefore, the Ce anomaly may not provide direct evidence of changes in redox conditions owing to the mineralogic control on REY abundance (*42*). There is a possibility that the transformation of Fe minerals releases more trivalent REY other than Ce, resulting in an intense negative Ce anomaly in pore water during the second REY-release event.

REY accumulation in bioapatite

In this study, there are commonly shallow (near SWI) and deep (>500 cmbsf) sinks for pore water REY following the two REY-release events (Fig. 2), indicating a postdepositional net uptake of REY from pore water by sediments. A possible reason for REY sink from pore water is diagenetic uptake by bioapatite, given that phosphate minerals are defined as the main REY host phase in REY-rich muds (*5*, *7*). The REY accumulations are considered to be generated by adsorption and/or substitution of REE^{3+} in the bioapatite crystal lattice (*43*, *44*), either through the substitutions $REE^{3+} + Si^{4+} \leftrightarrow Ca^{2+} + P^{5+}$ or $REE^{3+} + Na^{+} \leftrightarrow 2\ Ca^{2+}$, without forming REE minerals (*7*). The rapid increase in REY contents in each part of bioapatite fossils at shallow sediments (≤200 cm at GC062 site) (Fig. 7A) is in agreement with the idea that REY accumulation mainly takes place at the SWI where pore waters are still in communication with bottom water (*15*) and intensifies with depth (*8*). In situ laser ablation inductively coupled plasma mass spectrometry (ICP-MS) spot analysis reveals that the REY concentrations decrease significantly from the root (i.e., rim) part to the tip (i.e., inner) part of bioapatite (Fig. 7A). It is well known that the root part of fish teeth is prone to take up REY from the surrounding pore water during diagenesis (*7*, *15*). Because the dense enamel is impermeable to REY incorporation, the REY only diffuses into the fossil tooth via the entrance at the root part, resulting in the gradient of REY contents in bioapatite (*7*). The extremely high adsorption capacity of bioapatite crystals in the shallow subsurface results from the mineral component of fish teeth, which is thermodynamically metastable, and once exposed to pore water, the crystallites in fish teeth will react, dissolving or spontaneously recrystallizing, and increasing mean crystal sizes (*45*–*47*). Furthermore, crystal surfaces are exposed and tend to exchange with pore waters, as collagen that can limit interaction at the crystal surfaces degrades during early diagenesis (*7*, *46*). This superficial layer REY-enrichment mechanism can be attributed to the steep fall of REY near the SWI (Fig. 2) and the low sedimentation rate.

For fish teeth to survive into deep time, crystals need to grow, reducing their surface area and limiting intercrystalline porosity, which can effectively decrease the rate of REY exchange between bioapatite and pore waters (*46*–*48*), as evidenced by relatively constant REY contents in bioapatite in deeper sediments (≥200 cm at GC062 site) (Fig. 7A). In this case, REY can be gradually absorbed by bioapatite.

Implication for paleo-ocean environmental reconstruction

The REY geochemistry of bioapatite (i.e., REY distribution pattern and Ce anomaly) has been traditionally regarded as a robust proxy for reconstructing ancient seawater chemistry (*15*, *43*, *49*, *50*). Such reconstruction is connected to the preservation of seawater-like REE pattern in bioapatite due to immediate REY sequestration during

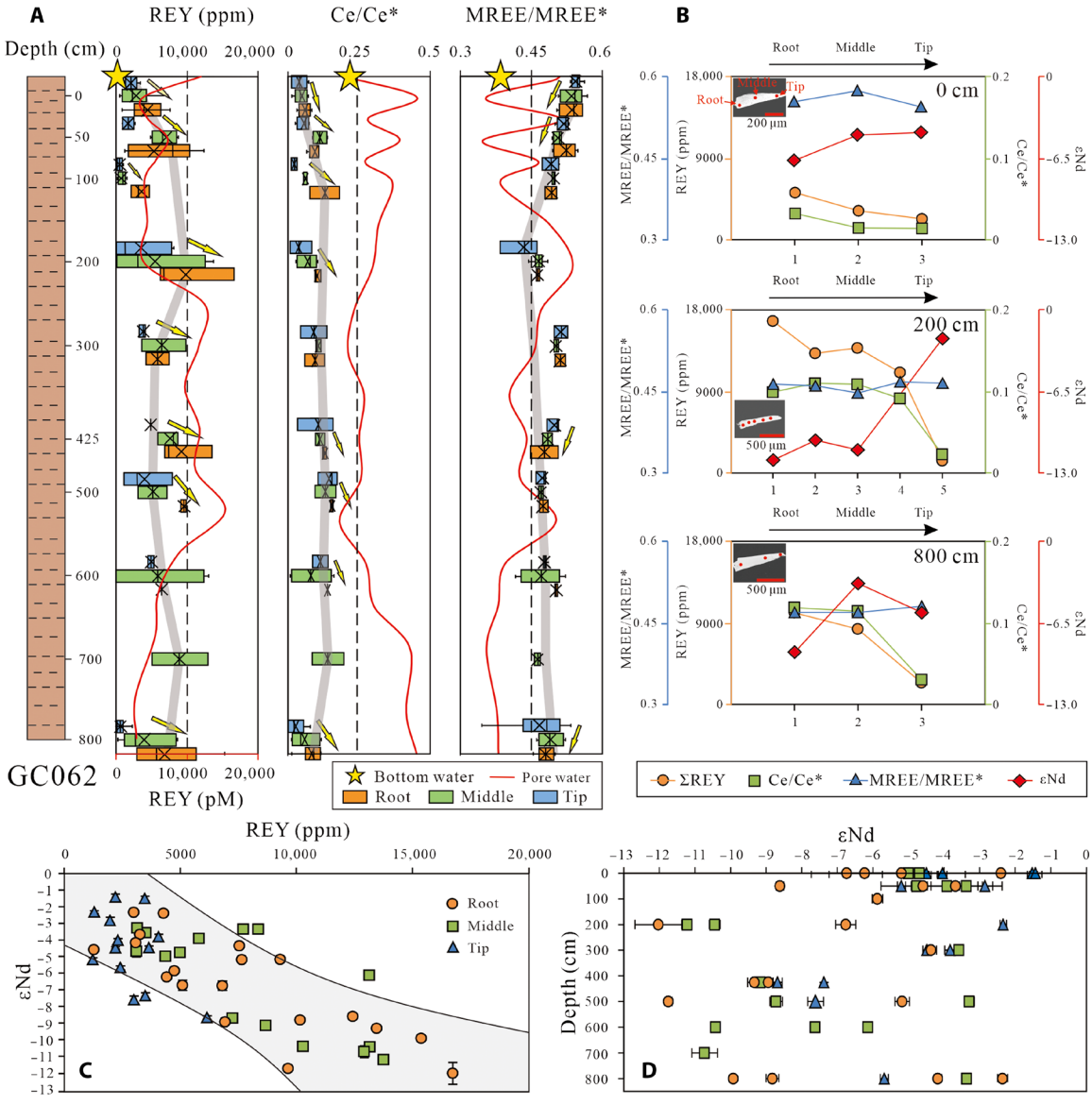

Fig. 7. Variations of REY, MREE/MREE*, Ce/Ce*, and εNd at root, middle, and tip in bioapatite. (**A**) Comparison of REY characteristics among bioapatite, pore water, and bottom seawater. (**B**) In situ compositional analysis showing the gradients of REY, Ce/Ce*, MREE/MREE*, and εNd in each part of bioapatite. (**C**) Binary cross-correlation plots of REY and εNd from root, middle, and tip in bioapatite. (**D**) εNd distribution in bioapatite with depth.

exposure at the SWI where pore waters are still in communication with the overlying water column (*15*, *27*). However, given the relatively slow rates of REY uptake (*11*), recent studies have indicated that the primary REY signal of bioapatite can be modified because it can continuously incorporate REY from ambient pore waters during diagenesis (*5*, *7*, *8*, *17*). MREE-enriched patterns are common in bioapatite (*16*, *17*, *51*), which might preserve pore water REY signatures due to observed minor fractionation during the incorporation of REY to bioapatite (*8*). Therefore, it is still unknown whether the REY of bioapatite fossil record pore water compositions directly or reveal REY fractionation during early diagenesis.

The pore water REY results show that, at GC120 site, the concentrations of LREE, MREE, and HREE decrease by 60, 51, and 45%, respectively, from the SWI to onset of the second REY-release event. The concentration of LREE, MREE, and HREE increased by 556, 641, and 441%, respectively, during the second REY-release event. These values decreased by 81, 84, and 83% respectively, in the lower part of the core. The same trend is observed at the other two sites, which indicates the existence of REY fractionation relative to sediment compositions. This is further supported by the variation of REY ratios and their crossplots. Figure 8 shows MREE and HREE concentrations plotted against LREE concentrations for pore water. LREE-MREE and LREE-HREE plots display relative linear relationships in the lower LREE concentration range, corresponding to the start of the second REY-release event and the bottom of the core where REY systematically decreases with depth. Substantial deviations in the LREE-MREE and LREE-HREE plots occur at the end of the second REY-release event (Fig. 8). Moreover, La_N/Yb_N, La_N/Sm_N,

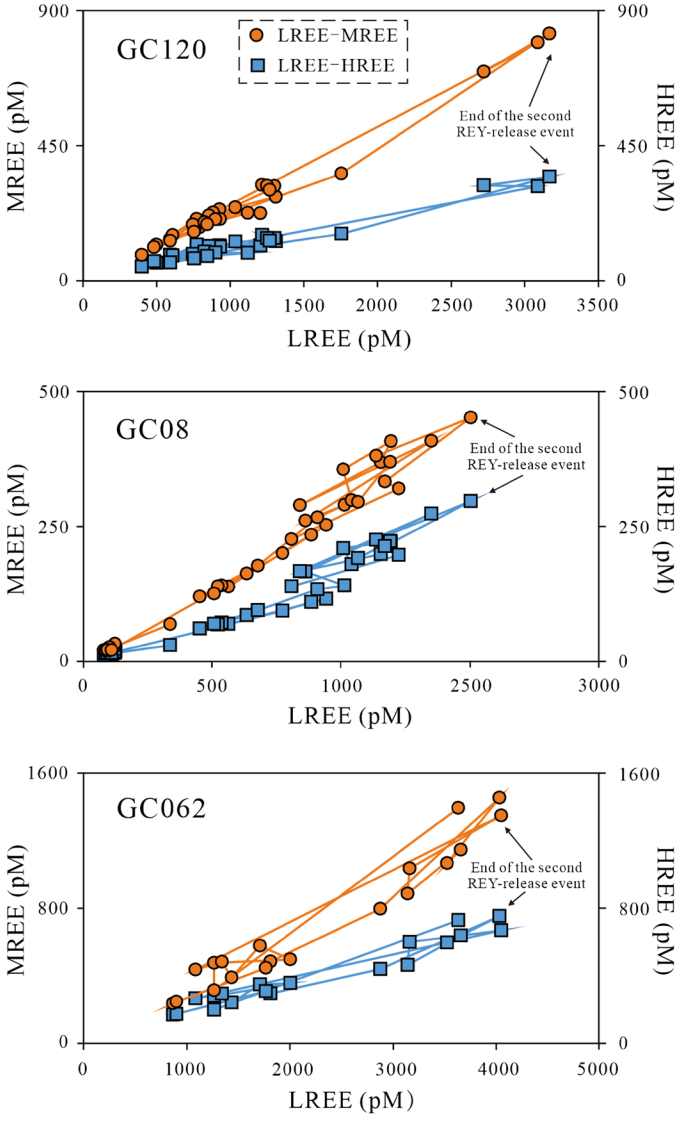

Fig. 8. MREE and HREE concentrations plotted against LREE concentrations of pore water.

and Sm_N/Yb_N can represent the ratios between LREE, MREE, and HREE (*18*). La_N/Sm_N ratios gradually fall in the second REY-release event with a further rise down the core, while Sm_N/Yb_N show the opposite trend, and La_N/Yb_N remains nearly constant at all sites. Systematic features of fractionation indicate that the LREE and MREE (especially MREE) are released more readily than the HREE, and MREE are selective and largely regenerated in the second REY-release event and then adsorbed on bioapatite in the lower part of the cores.

The bioapatite of the Holocene was reported to be characterized by modern seawater-like REE patterns with low REY contents (*19*). Conversely, Miocene and older bioapatite show more REY enrichment. For example, most Early Cenozoic and late Mesozoic bioapatite displays obvious MREE-enriched, MREE bulge–type pattern (*19*, *44*). These REY deviations are either attributed to secular variations of seawater chemistry in the geologic history (*19*, *50*) or more extensive diagenesis involving REY fractionation (*44*). Despite the REY patterns of bioapatite being approximately similar to seawater, the heterogeneous REY patterns and concentrations in such phosphate minerals are discernible at GC062 site (Fig. 7), indicating possible fractionation during diagenetic trapping in bioapatite. Most bioapatite fossils contain extremely high REY concentrations at the root part (as high as ~16,738 ppm; table S2) and show notable REY gradients from the root part to the tip part (Fig. 7, A and B). The dentine is much more permeable than dense enamel during diagenetic incorporation of REY, which get adsorbed onto the root via the breach from the pore water (*7*, *11*). The slightly higher MREE/MREE* values and lower Ce/Ce* values in the root part of bioapatite at the SWI relative to those of uppermost pore water and bottom water (Fig. 7A) further indicate that MREE and LREE (except for Ce) are progressively removed through preferential adsorption onto external surfaces of bioapatite from pore water. This slight fractionation is induced by the adsorption mechanism, controlled by surface crystal-chemical properties (*44*).

The linear enhancement of MREE/MREE* values and negative Ce anomaly and rapidly decreasing in REY from root to tip is observed within most individual fossil bioapatite (Fig. 7, A and B). The REY of inner portions of bioapatite is believed to derive from seawater and show much higher MREE/MREE* values and lower Ce/Ce* values compared to bottom seawater (Fig. 7A). Such linear enhancement demonstrates the intensity of REY fractionation from one another during diffusive transport and substitution within bioapatite (*44*, *46*, *52*). The substitution mechanism caused by bulk crystal-chemical properties results in relative ease of substituting REE ions of the different ionic radius into the Ca sites in the bioapatite lattice, which could be a potential contributor to fractionation with pore water (*46*).

It is worth noticing that the variations in REY, Ce/Ce*, and MREE in different areas both at the root and tip parts of bioapatite fossils tightly mirror those of surrounding pore waters, both of which show enormous differences from bottom water (Fig. 7A). These suggest that bioapatite REY geochemistry records neither seawater nor pore water but adsorption and desorption processes of REY during early diagenesis.

In addition, bioapatite displays an inhomogeneous distribution of εNd values that slightly increases from root to tip (Fig. 7B). The wide range of εNd between −12.0 and −1.4 (mean = −6.1) is comparable with previously published εNd data of bioapatite in REY-rich sediment (*53*, *54*). These results are significantly different from that of the Pacific Deep Water (−3.5) and the North Pacific Intermediate Water (−3.0) (*55*). The mechanism for the alteration of εNd in the fish teeth remains unknown. The Nd isotope compositions of fish teeth fossils have widely been used to trace paleoseawater compositions and past ocean circulation patterns (*15*, *27*, *49*), as the εNd value seems not to be changed during in vivo ingestion nor fractionated during postmortem REE incorporation (*56*). The reasonable explanation for the resistance of Nd isotopes to alteration is the low concentration of Nd in pore water relative to that in the mineral (*15*). However, diagenetic REY uptake can occur over prolonged time scales (millions of years) and may modify the bioapatite εNd value if the pore water has a different REY and Nd isotope composition (*15*, *56*). The modern fish teeth have Nd concentrations ~5 order lower than that of fossil bioapatite (*56*), which indicates that the chief source of Nd in bioapatite is from pore water. In this study, pore water shows extremely high REY concentrations and distinctive REY patterns relative to that of seawater (Fig. 2), which can introduce enough Nd into bioapatite under extremely low sedimentation

rates, affecting the original Nd isotopic ratios within bioapatite (*15*). Although the Nd isotopic compositions of pore water in REY-rich sediment remain unclear, εNd values are usually different between pore water and overlying water (*24*). The pore water εNd is determined by sediment diagenesis (*35*). Bioapatite εNd values are similar to those of the embedding sediment (*56*). The εNd values in REY-rich sediments in the Pacific Ocean show less radiogenic values (~−5.3) (*53*) relative to modern seawater (*55*). Meanwhile, ferromanganese sediment, a possible source of pore water Nd, displays lower εNd values than seawater (*53*). A weak negative correlation between εNd and REY occurs in each part of bioapatite fossils (Fig. 7C). Therefore, we infer that the original εNd values of bioapatite in deep-sea sediment may be altered by pore water with high Nd concentrations and low εNd values during diagenesis.

The diagenetic Nd uptake from the pore water (*56*) might contribute to the substantial variability in εNd values. In the water column, the εNd values of fish teeth tend to integrate seawater values (*15*, *27*, *53*). During postmortem diagenetic REY uptake into bioapatite within a few 10^4 years at the SWI, the εNd values of the root part of fish teeth may be affected (*56*) due to a 10^5-time increase in Nd concentrations (*7*). Bioapatite εNd seems unlikely to be changed significantly in a short time scale. This is confirmed by relatively high values of εNd in each part of bioapatite from shallow sediment (≤100 cmbsf) (Fig. 7D). In particular, the average value of εNd in the tip part of bioapatite is −3.3 (table S5), which can still preserve a seawater signal (*55*). With increasing depth in the sediment column, the second REY-release event introduces substantial Nd (Fig. 2) with a distinct εNd value into the pore water. Considering an extremely slow sedimentation rate in the study area (*26*), diagenetic Nd uptake in the fish teeth can occur over time scales of millions of years, resulting in further alteration of εNd in bioapatite (*15*, *56*). The εNd of the middle part and the tip part can be gradually affected during REY diagenetic substitution and diffusion processes in the bioapatite lattice. This interpretation is supported by the significantly low εNd values in each bioapatite part in deep sediment (≥100 cmbsf; Fig. 7D). These results indicate that the Nd isotopic signal in bioapatite has been likely blurred by diagenetic alteration, thus in turn recording a Nd isotopic signal of diagenetic processes.

MATERIALS AND METHODS

The seawater and sediment samples were collected on the ship using CTD (conductance, temperature, and depth) and gravity corer during the Guangzhou Marine Geological Survey Haiyang-6 Cruise in July 2017. All the bottles, samplers, tubing, and filters were cleaned with acid and Milli-Q water before use. The shipboard sampling procedures are described in detail in (*18*). Briefly, bottom water samples, approximately 25 m above the seafloor, were collected in Niskin bottles attached to an epoxy-coated CTD rosette. These samples were immediately filtered through 0.45-μm filter, stored in acid-washed high-density polyethylene bottles, and acidified to pH 2 using high-purity HCl. The pore water samples were collected immediately after the sediment collection to minimize the contact with ambient air. Briefly, high-resolution pore water samples were extracted by Rhizon sampling device (pore diameter of ~0.1 μm) in an anoxic environment. These samples were kept in precleaned polytetrafluoroethylene (PFA) tubes and acidified to pH ~ 2 using ultrapure HCl. Samples from Rhizons not only show accurate values of pH, sulfate, alkalinity, and metal concentrations but also yield good results of REY determination in pore water (*18*). All the aliquots and sediment samples were stored at 4°C before further analyses.

Water analyses

To avoid contamination, the experimental tools, including Teflon beakers, polypropylene bottles, and tubing, were cleaned by ultrapure acid and Milli-Q water. Ultraclean reagents (Thermo Fisher Scientific, optima grade) were used. The dissolved REY concentrations were analyzed by an online preconcentration system at Laboratory of Elemental Scientific Inc. (Shanghai, China) via an ICP-MS (Agilent 7900, CA, USA) coupled to an ESI SeaFAST III (automated preconcentration system for seawater; Elemental Scientific Inc., NE, USA). Sample preparation and measurements followed the procedure established by (*8*, *20*, *57*). This system is used to remove the water matrix and improve the sensitivity via an ion exchange column consisting of ethylenediaminetriacetic acid and iminodiacetic acid functional groups to selectively preconcentrate REY from water samples while washing out anions and alkali and alkaline earth cations at pH of ~7. The method used here used a 7-ml PFA sample loop that required an initial sample volume of approximately 8 ml. To assess the accuracy of this technique, seawater certified reference materials (CRMs) (NASS-6, National Research Council of Canada) were used as there is no CRM that exists for pore waters. The deviations between the REY results and the literature values are less than 10% (1σ) (table S6). The external accuracy based on replicate measurements (n = 10) of NASS-6 was ≤10% for all REY. Detection limits were assessed by three times of the signal of 1% HNO_3 blanks, which were between 0.016 and 0.88 pM. Although no shipboard procedural blanks were taken during this cruise, procedural blanks were determined in the laboratory, which were indistinguishable from 1% HNO_3 blank signals and were below the defined detection limits (table S6). The REY concentrations were normalized to PAAS (*58*); $Ce/Ce^* = Ce_N / (1/2La_N + 1/2Pr_N)$, $Eu/Eu^* = Eu_N / (1/2Sm_N + 1/2Gd_N)$, and $Y/Y^* = Y_N / (1/2Dy_N + 1/2Ho_N)$ were calculated (*18*); and MREE/MREE* = 2 × average (MREE) / [average (LREE) + average (HREE)] was calculated according to (*17*).

Dissolved Mn, Fe, and Al concentrations in pore water were performed on 50-fold diluted samples by Milli-Q water following the procedure established by (*18*). The precision was generally better than 10%. The concentrations of SO_4^{2-}, NO_3^-, Cl^-, Br^-, and F^- were measured using the ICS-1100 ion chromatograph (Thermo Fisher Scientific, MA, USA), following the procedures described by (*18*). Ion concentrations were determined on 100-fold diluted samples by ultrapure water. The AG19-type column was used for ion separation, and a bicarbonate solution (i.e., 1.8 mM Na_2CO_3 + 1.7 mM $NaHCO_3$) was used as the eluent. The relative SD for ions in samples was ≤1%. The concentrations of Mn, Fe, and the anion were measured at the Third Institute of Oceanography, State Oceanic Administration (Xiamen, China).

Sediment analyses

Sediment samples were crushed and pulverized (200 mesh). Preparation for REY analyses of sediment followed the method of (*18*). At first, 50-mg sample was weighed into a precleaned Teflon beaker, followed by addition of HCl, HF, and $HClO_4$. Subsequently, the mixture was evaporated to near dryness. Last, the residues were redissolved in 10% HNO_3 and diluted to 25 ml with double distilled water. REY was measured via ICP-MS (X-Series II, Thermo Fisher Scientific, MA, USA). The analytical precision was better than 5%.

Clay minerals were identified by x-ray diffraction (XRD) using a Rigaku diffractometer (D/Max 2500PC, Tokyo, Japan). Three XRD runs were performed, following air-drying, ethylene glycol solvation for 24 hours, and heating at 490°C for 2 hours. Semiquantitative estimates of peak areas of the basal reflections for the montmorillonite (including mixed layers) (15 to 17 Å) were carried out using the Jade software.

In situ elemental and Nd isotopic analyses

The typical fossil fish teeth samples were hand-picked from bulk sediments of 10 stratigraphic intervals [0, 50, 100, 200, 300, 425, 500, 600, 700, and 800 (cmbsf), respectively] by using a binocular microscope. These bioapatite samples were cleaned with Milli-Q water, then embedded in epoxy resin, and polished by diamond abrasive. As REY might be distributed heterogeneously within the tooth fossils (*7*), it is necessary to analyze the different parts of samples. On the basis of the morphological characteristics of fossil teeth divided into three parts with the same length from outer rim to inner, described as root, middle, and tip.

A 193-nm ArF excimer laser ablation system (RESOlution M-50, Resonetics, USA) coupled with either an ICP-MS (Element XR, Thermo Fisher Scientific, USA) or multicollector ICP-MS (Neptune, Thermo Fisher Scientific, USA) used for REY and Nd isotopic analysis, respectively. The REY abundant were normalized by NIST SRM 610 and the Ca content obtained by electron probe microanalysis was used as the internal standard. Data reduction was performed using ICPMSDataCal software.

In situ Nd isotopic analyses followed the method of (*53*). An X skimmer cone and a small N^2 (2 ml/liter) flow improved the instrumental sensitivity. The aerosol ablated by the laser gets transported using helium as a carrier gas (800 ml/min). The beam diameter and ablation frequency were 31 to 82 μm and 6 Hz, respectively. Before every analytical session, the instrument was configured to monitor Kr in the Ar gas after optimization. All isotope signals were detected with Faraday cups under static mode. Each analysis consisted of 250 cycles with an integration time of 0.262 s per cycle. The gas blank of ^{143}Nd was less than 0.2 mV. The mass bias of $^{143}Nd/^{144}Nd$ was normalized to $^{146}Nd/^{144}Nd = 0.7129$ with an exponential law. Analyses of 25 apatite Durango and 40 apatite McClure standard sample yielded a weighted mean of $^{143}Nd/^{144}Nd = 0.512470 \pm 0.000060$ (2SD) and $^{143}Nd/^{144}Nd = 0.512280 \pm 0.000055$ (2SD), respectively, which is identical within error to their published values. REY compositions and Nd isotopes were analyzed at Guangzhou Institute of Geochemistry, Chinese Academy of Sciences (Guangzhou, China). Nd isotopic analyses are reported in the standard epsilon notation $\varepsilon Nd(t) = [(^{143}Nd/^{144}Nd)_{sample}\ (t) / (^{143}Nd/^{144}Nd)_{CHUR}\ (t) - 1]10^4$, where CHUR is the chondritic uniform reservoir with a present day $^{143}Nd/^{144}Nd = 0.512638$.

SUPPLEMENTARY MATERIALS

Supplementary material for this article is available at https://science.org/doi/10.1126/sciadv.abn5466

REFERENCES AND NOTES

1. H. Elderfield, M. J. Greaves, The rare earth elements in seawater. *Nature* **296**, 214–219 (1982).
2. R. F. Service, Nations move to head off shortages of rare earths. *Science* **327**, 1596–1597 (2010).
3. C. Xu, J. Kynický, M. P. Smith, A. Kopriva, M. Brtnický, T. Urubek, Y. Yang, Z. Zhao, C. He, W. Song, Origin of heavy rare earth mineralization in south China. *Nat. Commun.* **8**, 14598 (2017).
4. Y. Kato, K. Fujinaga, K. Nakamura, Y. Takaya, K. Kitamura, J. Ohta, R. Toda, T. Nakashima, H. Iwamori, Deep-sea mud in the Pacific Ocean as a potential resource for rare-earth elements. *Nat. Geosci.* **4**, 535–539 (2011).
5. T. Kashiwabara, R. Toda, K. Nakamura, K. Yasukawa, K. Fujinaga, S. Kubo, T. Nozaki, Y. Takahashi, K. Suzuki, Y. Kato, Synchrotron x-ray spectroscopic perspective on the formation mechanism of REY-rich muds in the Pacific Ocean. *Geochim. Cosmochim. Acta* **240**, 274–292 (2018).
6. K. Yasukawa, J. Ohta, T. Miyazaki, B. S. Vaglarov, Q. Chang, K. Ueki, C. Toyama, J.-I. Kimura, E. Tanaka, K. Nakamura, K. Fujinaga, K. Iijima, H. Iwamori, Y. Kato, Statistic and isotopic characterization of deep-sea sediments in the western north Pacific Ocean: Implications for genesis of the sediment extremely enriched in rare earth elements. *Geochem. Geophy. Geosy.* **20**, 3402–3430 (2019).
7. J. Liao, X. Sun, D. Li, R. Sa, Y. Lu, Z. Lin, L. Xu, R. Zhan, Y. Pan, H. Xu, New insights into nanostructure and geochemistry of bioapatite in REE-rich deep-sea sediments: LA-ICP-MS, TEM, and Z-contrast imaging studies. *Chem. Geol.* **521**, 58–68 (2019).
8. S. A. L. Paul, J. B. Volz, M. Bau, M. Köster, S. Kasten, A. Koschinsky, Calcium phosphate control of REY patterns of siliceous-ooze-rich deep-sea sediments from the central equatorial Pacific. *Geochim. Cosmochim. Acta* **251**, 56–72 (2019).
9. J. Liao, J. Chen, X. Sun, Z. Wu, Y. Deng, X. Shi, Y. Wang, Y. Chen, A. Koschinsky, Quantifying the controlling mineral phases of rare-earth elements in deep-sea pelagic sediments. *Chem. Geol.* **595**, 120792 (2022).
10. A. Menendez, R. H. James, S. Roberts, K. Peel, D. Connelly, Controls on the distribution of rare earth elements in deep-sea sediments in the north Atlantic Ocean. *Ore Geol. Rev.* **87**, 100–113 (2017).
11. K. Toyoda, M. Tokonami, Diffusion of rare-earth elements in fish teeth from deep-sea sediments. *Nature* **345**, 607–609 (1990).
12. K. C. Ruttenberg, Development of a sequential extraction method for different forms of phosphorus in marine sediments. *Limnol. Oceanogr.* **37**, 1460–1482 (1992).
13. P. Kraal, N. Dijkstra, T. Behrends, C. P. Slomp, Phosphorus burial in sediments of the sulfidic deep Black Sea: Key roles for adsorption by calcium carbonate and apatite authigenesis. *Geochim. Cosmochim. Acta* **204**, 140–158 (2017).
14. C. R. German, G. P. Klinkhammer, J. M. Edmond, A. Mura, H. Elderfield, Hydrothermal scavenging of rare-earth elements in the ocean. *Nature* **345**, 516–518 (1990).
15. E. E. Martin, H. D. Scher, Preservation of seawater Sr and Nd isotopes in fossil fish teeth: Bad news and good news. *Earth Planet. Sci. Lett.* **220**, 25–39 (2004).
16. C. A. Bright, A. M. Cruse, T. W. Lyons, K. G. Macleod, M. D. Glascock, R. L. Ethington, Seawater rare-earth element patterns preserved in apatite of Pennsylvanian conodonts? *Geochim. Cosmochim. Acta* **73**, 1609–1624 (2009).
17. J. Chen, T. J. Algeo, L. Zhao, Z. Q. Chen, L. Cao, L. Zhang, Y. Li, Diagenetic uptake of rare earth elements by bioapatite, with an example from Lower Triassic conodonts of South China. *Earth-Sci. Rev.* **149**, 181–202 (2015).
18. Y. Deng, J. Ren, Q. Guo, J. Cao, H. Wang, C. Liu, Rare earth element geochemistry characteristics of seawater and porewater from deep sea in western pacific. *Sci. Rep.* **7**, 16539 (2017).
19. J. Wright, H. Schrader, W. T. Holser, Paleoredox variations in ancient oceans recorded by rare earth elements in fossil apatite. *Geochim. Cosmochim. Acta* **51**, 631–644 (1987).
20. A. N. Abbott, A benthic flux from calcareous sediments results in nonconservative neodymium behavior during lateral transport: A study from the Tasman Sea. *Geology* **47**, 363–366 (2019).
21. E. R. Sholkovitz, D. J. Piepgras, S. B. Jacobsen, The pore water chemistry of rare earth elements in Buzzards Bay sediments. *Geochim. Cosmochim. Acta* **53**, 2847–2856 (1989).
22. E. R. Sholkovitz, T. J. Shaw, D. L. Schneider, The geochemistry of rare earth elements in the seasonally anoxic water column and porewaters of Chesapeake Bay. *Geochim. Cosmochim. Acta* **56**, 3389–3402 (1992).
23. B. A. Haley, G. P. Klinkhammer, J. McManus, Rare earth elements in pore waters of marine sediments. *Geochim. Cosmochim. Acta* **68**, 1265–1279 (2004).
24. A. N. Abbott, B. Haley, J. McManus, Bottoms up: Sedimentary control of the deep North Pacific Ocean's εNd signature. *Geology* **43**, 1035–1038 (2015).
25. A. N. Abbott, B. Haley, J. McManus, C. Reimers, The sedimentary flux of dissolved rare earth elements to the ocean. *Geochim. Cosmochim. Acta* **154**, 186–200 (2015).
26. Y. P. Lancelot, R. Larson, A. Fisher, L. Abrams, R. Behl, W. H. Busch, G. Cameron, P. R. Castillo, J. M. Covington, G. Dürr, E. Erba, P. A. Floyd, C. France~Lanord, E. H. Hauser, S. M. Karl, A.-M. Karpoff, A. Matsuoka, A. Molinie, J. G. Ogg, A.R.M. Salimullah, M. Steiner, B. P. Wallick, W. Wightman, Site 800. *Proc. Ocean Drill. Prog. Init. Res.* **129**, 33–89 (1990).
27. S. Felitsyn, U. Sturesson, L. Popov, L. Holmer, Nd isotope composition and rare earth element distribution in early Paleozoic biogenic apatite from Baltoscandia: A signature of Iapetus ocean water. *Geology* **26**, 1083–1086 (1998).
28. E. R. Sholkovitz, W. M. Landing, B. L. Lewis, Ocean particle chemistry: The fractionation of rare earth elements between suspended particles and seawater. *Geochim. Cosmochim. Acta* **58**, 1567–1579 (1994).
29. H. J. W. De Baar, C. R. German, H. Elderfield, P. Van Gaans, Rare earth element distributions in anoxic waters of the Cariaco Trench. *Geochim. Cosmochim. Acta* **52**, 1203–1219 (1988).

30. A. N. Abbott, S. Löhr, M. Trethewy, Are clay minerals the primary control on the oceanic rare earth element budget? *Front. Mar. Sci.* **6**, 504 (2019).
31. L. A. Anderson, J. L. Sarmiento, Global ocean phosphate and oxygen simulations. *Glob. Biogeochem. Cycles* **9**, 621–636 (1995).
32. H. Røy, J. Kallmeyer, R. R. Adhikari, R. Pockalny, B. B. Jørgensen, S. D'Hondt, Aerobic microbial respiration in 86-million-year-old deep-sea red clay. *Science* **336**, 922–925 (2012).
33. S. D'Hondt, B. B. Jørgensen, D. J. Miller, A. Batzke, R. Blake, B. A. Cragg, H. Cypionka, G. R. Dickens, T. Ferdelman, K. U. Hinrichs, N. G. Holm, R. Mitterer, A. Spivack, G. Z. Wang, B. Bekins, B. Engelen, K. Ford, G. Gettemy, S. D. Rutherford, H. Sass, C. G. Skilbeck, I. W. Aiello, G. Guèrin, G. H. House, F. Inagaki, P. Meister, T. Naehr, S. Niitsuma, R. J. Parkes, A. Schippers, D. C. Smith, A. Teske, J. Wiegel, C. N. Padilla, J. L. S. Acosta, Distributions of microbial activities in deep subseafloor sediments. *Science* **306**, 2216–2221 (2004).
34. S. D'Hondt, F. Inagaki, C. A. Zarikian, L. J. Abrams, N. Dubois, T. Engelhardt, H. Evans, T. Ferdelman, B. Gribsholt, R. N. Harris, B. W. Hoppie, J. H. Hyun, J. Kallmeyer, J. Kim, J. E. Lynch, C. C. McKinley, S. Mitsunobu, Y. Morono, R. W. Murray, R. Pockalny, J. Sauvage, T. Shimono, F. Shiraishil, D. C. Smith, C. E. Smith-Duque, A. J. Spivack, B. O. Steinsbu, Y. Suzuki, M. Szpak, L. Toffin, G. Uramoto, Y. T. Yamaguchi, G. L. Zhang, X. H. Zhang, W. Ziebis, Presence of oxygen and aerobic communities from sea floor to basement in deep-sea sediments. *Nat. Geosci.* **8**, 299–304 (2015).
35. A. N. Abbott, B. A. Haley, J. McManus, The impact of sedimentary coatings on the diagenetic Nd flux. *Earth Planet. Sci. Lett.* **449**, 217–227 (2016).
36. J. Kim, M. E. Torres, B. A. Haley, M. Kastner, J. W. Pohlman, M. Riedel, Y. Lee, The effect of diagenesis and fluid migration on rare earth element distribution in pore fluids of the northern Cascadia accretionary margin. *Chem. Geol.* **291**, 152–165 (2012).
37. T. O. Soyol-Erdene, Y. Huh, Rare earth element cycling in the pore waters of the Bering Sea Slope (IODP Exp. 323). *Chem. Geol.* **358**, 75–89 (2013).
38. S. W. Poulton, D. E. Canfield, Co-diagenesis of iron and phosphorus in hydrothermal sediments from the southern east pacific rise: Implications for the evaluation of paleoseawater phosphate concentrations. *Geochim. Cosmochim. Acta* **70**, 5883–5898 (2006).
39. J. R. Hein, H. W. Yeh, E. Alexander, Origin of iron-rich montmorillonite from the manganese nodule belt of the north equatorial pacific. *Clays Clay Miner.* **27**, 185–194 (1979).
40. H. Elderfield, E. R. Sholkovitz, Rare earth elements in the pore waters of reducing nearshore sediments. *Earth Planet. Sci. Lett.* **82**, 280–288 (1987).
41. L. S. Prakash, D. Ray, A. L. Paropkari, A. V. Mudholkar, M. Satyanarayanan, B. Sreenivas, D. Chandrasekharam, D. Kota, K. A. K. Raju, S. Kaisary, V. Balaram, T. Gurav, Distribution of REEs and yttrium among major geochemical phases of marine Fe–Mn-oxides: Comparative study between hydrogenous and hydrothermal deposits. *Chem. Geol.* **312-313**, 127–137 (2012).
42. E. H. De Carlo, Paleoceanographic implications of rare earth element variability within a Fe-Mn crust from the central Pacific Ocean. *Mar. Geol.* **98**, 449–467 (1991).
43. H. D. Scher, E. E. Martin, Timing and climatic consequences of the opening of Drake Passage. *Science* **312**, 428–430 (2006).
44. B. Reynard, C. Lécuyer, P. Grandjean, Crystal–chemical controls on rare-earth element concentrations in fossil biogenic apatites and implications for paleoenvironmental reconstructions. *Chem. Geol.* **155**, 233–241 (1999).
45. F. Berna, A. Matthews, S. Weiner, Solubilities of bone mineral from archaeological sites: The recrystallization window. *J. Archaeol. Sci.* **31**, 867–882 (2004).
46. C. N. Trueman, L. Kocsis, M. R. Palmer, C. Dewdney, Fractionation of rare earth elements within bone mineral: A natural cation exchange system. *Palaeogeogr. Palaeoclimatol. Palaeoecol.* **310**, 124–132 (2011).
47. J. Moradian-Oldak, S. Weiner, L. Addadi, W. J. Landis, W. Traub, Electron imaging and diffraction study of individual crystals of bone, mineralized tendon and synthetic carbonate apatite. *Connect. Tissue Res.* **25**, 219–228 (1991).
48. L. Kocsis, C. N. Trueman, M. Palmer, Protracted diagenetic alteration of REE contents in fossil bioapatites: Direct evidence from Lu-Hf isotope systematics. *Geochim. Cosmochim. Acta* **74**, 6077–6092 (2010).
49. E. E. Martin, B. A. Haley, Fossil fish teeth as proxies for seawater Sr and Nd isotopes. *Geochim. Cosmochim. Acta* **64**, 835–847 (2000).
50. S. Picard, C. Le'cuyer, J. A. Barrat, J. P. G. G. Dromart, S. M. F. Sheppard, Rare earth element contents of Jurassic fish and reptile teeth and their potential relation to seawater composition (Anglo-Paris Basin, France and England). *Chem. Geol.* **186**, 1–16 (2002).
51. G. A. Shields, G. E. Webb, Has the REE composition of seawater changed over geological time? *Chem. Geol.* **204**, 103–107 (2004).
52. C. A. Suarez, G. MacPherson, L. Gonzalez, D. Grandstaff, Heterogeneous rare earth element (REE) patterns and concentrations in a fossil bone: Implications for the use of REE in vertebrate taphonomy and fossilization history. *Geochim. Cosmochim. Acta* **74**, 2970–2988 (2010).
53. T. C. Zhou, X. F. Shi, M. Huang, M. Yu, D. J. Bi, X. W. Ren, J. H. Liu, A. M. Zhu, X. S. Fang, M. J. Shi, Genesis of REY-rich deep-sea sediments in the Tiki Basin, eastern South Pacific Ocean: Evidence from geochemistry, mineralogy and isotope systematics. *Ore Geo. Rev.* **138**, 104330 (2021).
54. F. L. Wang, G. W. He, X. G. Deng, Y. Yang, J. B. Ren, Fish teeth Sr isotope stratigraphy and Nd isotope variations: New insights on REY enrichments in deep-Sea sediments in the Pacific. *J. Mar. Sci. Eng.* **9**, 1379 (2021).
55. B. A. Haley, M. Frank, E. Hathorne, N. Pisias, Biogeochemical implications from dissolved rare earth element and Nd isotope distributions in the Gulf of Alaska. *Geochim. Cosmochim. Acta* **126**, 455–474 (2014).
56. T. Tutken, T. W. Vennemann, H. U. Pfretzschner, Nd and Sr isotope compositions in modern and fossil bones – Proxies for vertebrate provenance and taphonomy. *Geochim. Cosmochim. Acta* **75**, 5951–5970 (2011).
57. E. C. Hathorne, B. Haley, T. Stichel, P. Grasse, M. Zieringer, M. Frank, Online preconcentration ICP-MS analysis of rare earth elements in seawater. *Geochem. Geophys. Geosyst.* **13**, Q01020 (2012).
58. S. M. Mclennan, Relationships between the trace element composition of sedimentary rocks and upper continental crust. *Geochemistry Geophys. Geosystems* **2**, 2000GC000109 (2001).
59. T. Himmler, B. A. Haley, M. E. Torres, G. P. Klinkhammer, G. Bohrmann, J. Peckmann, Rare earth element geochemistry in cold-seep pore waters of hydrate ridge, northeast Pacific Ocean. *Geo-Mar. Lett.* **33**, 369–379 (2013).
60. M. Raso, P. Censi, F. Saiano, Simultaneous determinations of zirconium, hafnium, yttrium and lanthanides in seawater according to a co-precipitation technique onto iron-hydroxide. *Talanta* **116**, 1085–1090 (2013).

Acknowledgments: We thank the crew and scientists of the vessel of Haiyangdizhi-6. We appreciate G. Shields, L. Famiyeh, Y. Hu, and M. Zhao for reviewing this manuscript. **Funding:** This research was financially supported by the National Natural Science Foundation of China (nos. 41803026, 41606048, 91958202, 42002085, 42072324, 41625006, and 41890824), Key Special Project for Introduced Talents Team of Southern Marine Science and Engineering Guangdong Laboratory (Guangzhou) (GML2019ZD0506), China Geological Survey Project (DD20190230 and DD20190629), the China Ocean Mineral Resources R&D Association (programs: DY135-C1-1-04), and Key Laboratory of Marine Mineral Resources, Ministry of Natural Resources (no. KLMMR-2015-A-03). **Author contributions:** Y.D. and Q.G. conceived the project. G.H., Congqiang Liu, and H.Q. supervised the project. Chenhui Liu, J.C., J.L., and H.W. collected the samples. Jianhou Zhou, Y.L., F.W., B.Z., R.W., and Jiang Zhu analyzed the samples. All authors contributed to the interpretation of the data and preparation of the manuscript. **Competing interests:** The authors declare that they have no competing interests. **Data and materials availability:** All data needed to evaluate the conclusions in the paper are present in the Supplementary Materials.

Submitted 5 December 2021
Accepted 5 May 2022
Published 22 June 2022
10.1126/sciadv.abn5466